

See discussions, stats, and author profiles for this publication at: <https://www.researchgate.net/publication/26750002>

# Perfluorinated Surfactant Chain-Length Effects on Sonochemical Kinetics

ARTICLE *in* THE JOURNAL OF PHYSICAL CHEMISTRY A · SEPTEMBER 2009

Impact Factor: 2.69 · DOI: 10.1021/jp903003w · Source: PubMed

---

CITATIONS

17

---

READS

85

4 AUTHORS, INCLUDING:



**Chad Vecitis**

Harvard University

51 PUBLICATIONS 1,399 CITATIONS

SEE PROFILE



**Michael R. Hoffmann**

California Institute of Technology

379 PUBLICATIONS 30,162 CITATIONS

SEE PROFILE

# Perfluorinated Surfactant Chain-Length Effects on Sonochemical Kinetics

Tammy Y. Campbell,<sup>†</sup> Chad D. Vecitis,<sup>†,§</sup> Brian T. Mader,<sup>‡</sup> and Michael R. Hoffmann<sup>\*,†</sup>

W. M. Keck Laboratories, California Institute of Technology, Pasadena, California 91125, and 3M Environmental Laboratories, 3M Center, Building 260-05-N-17, Maplewood, Minnesota 55144-1000

Received: April 1, 2009; Revised Manuscript Received: June 27, 2009

The sonochemical degradation kinetics of the aqueous perfluorochemicals (PFCs) perfluorobutanoate (PFBA), perfluorobutanesulfonate (PFBS), perfluorohexanoate (PFHA), and perfluorohexanesulfonate (PFHS) have been investigated. Surface tension measurements were used to evaluate chain-length effects on equilibrium air–water interface partitioning. The PFC air–water interface partitioning coefficients,  $K_{\text{eq}}^{\text{PF}}$ , and maximum surface concentrations,  $\Gamma_{\text{max}}^{\text{PF}}$ , were determined from the surface pressure equation of state for PFBA, PFBS, PFHA, and PFHS. Relative  $K_{\text{eq}}^{\text{PF}}$  values were dependent upon chain length  $K_{\text{eq}}^{\text{PFHS}} \cong 2.1K_{\text{eq}}^{\text{PFHA}} \cong 3.9K_{\text{eq}}^{\text{PFBS}} \cong 5.0K_{\text{eq}}^{\text{PFBA}}$ , whereas relative  $\Gamma_{\text{max}}^{\text{PF}}$  values had minimal chain length dependence  $\Gamma_{\text{max}}^{\text{PFHS}} \cong \Gamma_{\text{max}}^{\text{PFHA}} \cong \Gamma_{\text{max}}^{\text{PFBS}} \cong 2.2\Gamma_{\text{max}}^{\text{PFBA}}$ . The rates of sonolytic degradation were determined over a range of frequencies from 202 to 1060 kHz at dilute ( $<1 \mu\text{M}$ ) initial PFC concentrations and are compared to previously reported results for their  $\text{C}_8$  analogs: perfluorooctanesulfonate (PFOS) and perfluorooctanoate (PFOA). Under all conditions, the time-dependent PFC sonolytic degradation was observed to follow pseudo-first-order kinetics, i.e., below kinetic saturation, suggesting bubble–water interface populations were significantly below the adsorption maximum. The PFHX (where X = A or S) sonolysis rate constant was observed to peak at an ultrasonic frequency of 358 kHz, similar to that for PFOX. In contrast, the PFBX degradation rate constants had an apparent maximum at 610 kHz. Degradation rates observed for PFHX are similar to previously determined PFOX rates,  $k_{\text{app},358}^{\text{PFOX}} \cong k_{\text{app},358}^{\text{PFHX}}$ . PFOX is sonolytically pyrolyzed at the transiently cavitating bubble–water interface, suggesting that rates should be proportional to equilibrium interfacial partitioning. However, relative equilibrium air–water interfacial partitioning predicts that  $K_{\text{eq}}^{\text{PFOX}} \cong 5K_{\text{eq}}^{\text{PFHX}}$ . This suggests that at dilute PFC concentrations, adsorption to the bubble–water interface is ultrasonically enhanced due to high-velocity radial bubble oscillations. PFC sonochemical kinetics are slower for PFBS and further diminished for PFBA as compared to longer analogs, suggesting that PFBX surface films are of lower stability due to their greater water solubility.

## Introduction

Fluorinated surfactants, a subset of fluorochemicals (FCs), are composed of a hydrophobic, per- or polyfluorinated organic tail and highly water-soluble headgroup. Perfluorination, the replacement of all hydrogens with fluorines, imparts these compounds with unique physical properties such as great chemical inertness, minimal coefficients of friction, and low polarizabilities (i.e., hydro- and oleophobicity or fluorophilicity), making them desirable for a wide variety of commercial applications.<sup>1</sup> FCs are commonly employed to waterproof textiles and paper products, to protectively coat metals, as high-temperature lubricants,<sup>2</sup> in fire retardants such as aqueous film-forming foams (AFFF)<sup>3</sup> and in semiconductor processing.

Development of aqueous FC remediation technologies is of interest because of the environmental persistence of many PFCs, which has led to their global distribution in the environment and the presence of some FCs in human<sup>4</sup> and wildlife<sup>5,6</sup> plasma. Recent studies have detected low levels of perfluorobutanoate (PFBS) in marine wildlife of Western Europe,<sup>7</sup> but at significantly lower levels than PFOS and PFOA. Similar to PFOX, PFHX and PFBX are recalcitrant toward most conventional

wastewater remediation strategies.<sup>10,11</sup> Shortening of the hydrophobic tail increases water solubility. Accordingly, PFBS and PFBA exhibit a lower activity toward adsorption based removal techniques such as granular activated carbon (GAC),<sup>12</sup> which is currently used to remove PFOS and PFOA from pretreated wastewater streams.<sup>13</sup>

Sonochemistry has been reported to be effective for the destruction of PFOS and PFOA over a range of initial concentrations. High C–F bond dissociation energies ( $450\text{--}530 \text{ kJ mol}^{-1}$ ), C–C bond strengthening due to fluorination ( $\sim 14\text{--}17 \text{ kJ mol}^{-1}$  per fluorine atom), and the great one-electron reduction potential of fluorine ( $E^0 = 3.6 \text{ V}$ ) highlights the importance of high cavitation temperatures toward the degradation of fluorochemicals.<sup>14,15</sup> Interfacial temperatures produced by a transient bubble collapse provides sufficient energy for the thermolytic decomposition of FCs.<sup>16</sup> Initially, the C–C or C–S bond between the fluorocarbon tail and carboxylate or sulfonate headgroup is cleaved yielding a fluorochemical intermediate of high Henry's constant that migrates to the bubble core for further thermal and radical decomposition.<sup>17–19</sup> Consequently, aqueous solutions of PFOS and PFOA are readily mineralized during ultrasonic irradiation to their inorganic constituents:  $\text{F}^-$ ,  $\text{SO}_4^{2-}$ , CO, and  $\text{CO}_2$ .<sup>16,17</sup>

Acoustic cavitation events are responsible for the chemistry observed during ultrasonic irradiation of aqueous solutions. Cavitation occurs due to the acoustically driven growth (low P) and subsequent collapse (high P) of preexisting aqueous bubbles at ambient temperatures and pressures.<sup>16</sup> The transient

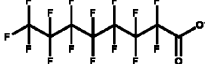
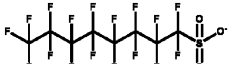
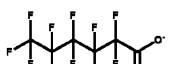
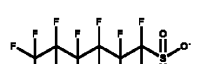
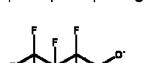
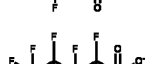
\* To whom correspondence should be addressed. E-mail: mrh@caltech.edu.

<sup>†</sup> California Institute of Technology. E-mail: T.Y.C., tcampbel@caltech.edu; C.D.V., vecitis@caltech.edu.

<sup>‡</sup> 3M Environmental Laboratories. E-mail: bmader@mmm.com.

<sup>§</sup> Current address: Department of Chemical Engineering, Environmental Engineering Program, Yale University, P.O. Box 208286, New Haven, CT 06520-8286.

TABLE 1: Physicochemical Properties of Perfluorinated Surfactants

Abbreviation	Name	Chemical Formula	Chemical Structure of the anionic form	M.W. (g mol <sup>-1</sup> )	Tail Carbons	pKa	Water Solubility (g L <sup>-1</sup> )	P <sub>vapor</sub> (Pa @ 20 °C)
PFOA-A	ammonium perfluorooctanoate	C <sub>8</sub> F <sub>15</sub> O <sub>2</sub> NH <sub>4</sub>		431	7	-0.1	9.5 <sup>b</sup>	9.3 x 10 <sup>-3 c</sup>
PFOS-K	potassium perfluorooctane sulfonate	C <sub>8</sub> F <sub>17</sub> SO <sub>3</sub> K		538	8	-3.27	0.5 <sup>d</sup>	3.3 x 10 <sup>-4 c</sup>
PFHA-A	ammonium perfluorohexanoate	C <sub>6</sub> F <sub>11</sub> O <sub>2</sub> NH <sub>4</sub>		331	5	N/A <sup>e</sup>	N/A	N/A
PFHS-K	potassium perfluorohexane sulfonate	C <sub>6</sub> F <sub>13</sub> SO <sub>3</sub> K		438	6	N/A	1.4	N/A
PFBA-A	ammonium perfluorobutanoate	C <sub>4</sub> F <sub>7</sub> O <sub>2</sub> NH <sub>4</sub>		231	3	0.4 <sup>b</sup>	N/A	<1.2 x 10 <sup>-5 a</sup>
PFBS-K	potassium perfluorobutane sulfonate	C <sub>4</sub> F <sub>9</sub> SO <sub>3</sub> K		338	4	N/A	46.2	N/A

<sup>a</sup> See ref 10. <sup>b</sup> See ref 56. <sup>c</sup> See ref 57. <sup>d</sup> See ref 58. <sup>e</sup> N/A = Data not available.

collapse of cavitation bubbles is quasi-adiabatic, heating the vapor phase inside the cavity to temperatures of 4000–5000 K, and yielding pressures on the order of 1000 bar.<sup>20–24</sup> Bubble–water interfacial temperatures have been estimated to be 500–1000 K.<sup>21,25</sup> As a direct consequence of these transient, localized high temperatures and pressures, solutes that have partitioned into the vapor phase or to the bubble–water interface is pyrolytically decomposed to various extents. Water vapor within the collapsing cavity is homolytically cleaved generating hydroxyl radicals, O-atoms and hydrogen atoms.<sup>23,26</sup> The radicals can also degrade organics in the bubble vapor, at the bubble–water interface and even in bulk aqueous solution.

Sonochemical degradation kinetics are a rough function of the physicochemical properties of an organic compound. The physicochemical properties of a compound can be used to evaluate relative partitioning to the (1) bubble vapor, (2) bubble–water interface, and (3) bulk aqueous phase in an ultrasonically irradiated solution, which are of decreasing sonochemical intensity. Listed in Table 1 are the physicochemical properties of perfluorinated surfactants of various chain lengths and headgroups: PFOS, PFOA, PFHS, PFHA, PFBS, and PFBA. The perfluorinated surfactants will preferentially adsorb to the air–water interface since they consist of a hydrophobic tail and a hydrophilic ionic headgroup. PFOS and PFOA have been shown to sonochemically decompose via pyrolytic reactions at the bubble–water interface. Thus, the sonolytic degradation rate will be proportional to the fraction of total surfactant molecules that adsorb to the interface of the transiently cavitating bubbles.<sup>27,28</sup> However, estimation of the fraction of total surfactant molecules adsorbed to transiently cavitating bubbles is difficult due to high-velocity bubble radial oscillations (>5 m/s) and short bubble lifetimes (<100 μs), which preclude utilization of equilibrium partitioning values.

A number of previous studies have evaluated surfactant adsorption to acoustic cavitation bubbles. Fyrrillas and Szeri used numerical simulations to show that high-velocity bubble oscillations drive an increased number of surfactant molecules to lightly populated interfaces while radial and thus surface area

minimums limited the maximum interfacial surfactant concentration.<sup>29</sup> Sostaric and Reisz determined that radical scavenging efficiency increases at high (>1 mM) surfactant concentrations with decreasing n-alkyl chain length in order of SPSO (sodium 1-pentanesulfonic acid) > SOS (sodium n-octanesulfate) ~ SOSO (sodium 1-octanesulfonic acid) > SDS (sodium dodecyl sulfate) or that the sonolytic rate maxima of nonvolatile alkyl surfactants does not correlate with the Gibbs surface excess.<sup>30</sup> Their results indicated that the Gibbs surface excess under ultrasonic irradiation was lower than the equilibrium surface excess. Acoustic emission spectra studies by Greiser and Ashokkumar reveal reduction of bubble coalescence and bubble clustering upon increasing SDS concentrations to 0.5–2 mM due to accumulation of anionic surfactants and thus negative charge at the bubble–water interface.<sup>31</sup>

Recently, FC surfactant sonochemistry has been investigated in a few studies. Moriwaki et al. determined that both PFOS and PFOA (PFOX where X = A or S) could be degraded sonochemically and that decomposition likely occurred via a bubble–water interface pyrolysis mechanism.<sup>16</sup> A detailed investigation into the PFOX time-dependent sonochemical products showed that after the initial decomposition step, PFOX was quickly converted into F<sup>-</sup>, SO<sub>4</sub><sup>2-</sup>, CO, and CO<sub>2</sub>.<sup>17</sup> In both cases, PFOA was sonochemically degraded faster than PFOS, consistent with perfluoroalkancarboxylates having a lower thermal activation energy than perfluoroalkanesulfonates; see ref 17 for mechanistic details. Modeling PFOX concentration-dependent kinetics using Langmuir–Hinshelwood kinetics indicated an enhancement of PFOS and PFOA bubble–water interface partitioning at low (<10 μM) concentrations due to high-velocity radial oscillations.<sup>32</sup> This was consistent with the results of Cheng et al. who observed that addition of relatively high (>10 mM) concentrations of semivolatile organics did not affect dilute PFOS and PFOA (<1 μM) sonochemical rates.<sup>33</sup>

Here, we investigate the ultrasonic degradation kinetics of dilute aqueous (<1 μM) solutions of the perfluorochemicals PFHS, PFHA, PFBA and PFBS. The results here are compared to the previously reported sonochemical kinetics of PFOS and

PFOA, such that the effects of PFC chain length ( $C_3$ – $C_8$ ) and headgroup ( $-\text{CO}_2^-$  vs  $-\text{SO}_3^-$ ) on kinetics can be evaluated. The FC sonochemical degradation rate chain-length dependence is compared to their equilibrium air–water interface partitioning chain-length dependence, as determined by surface tension measurements. The physical processes that govern sonochemical kinetics for dilute FCs and how these processes are affected by acoustic frequency are discussed.

### Experimental Methods

Perfluorobutyric acid (PFBA) and perfluorohexanoic acid (PFHA) were purchased from Sigma Aldrich. Potassium perfluorobutane-1-sulfonate (PFBS) and potassium perfluorohexane-1-sulfonate (PFHS) were provided by 3M. Ammonium acetate (>99%) and methanol (HR-GC > 99.99%) were obtained from EMD Chemicals Inc. Aqueous solutions were prepared with purified water using a Milli-Q system (18.2 M $\Omega$  cm resistivity). Acid solutions were brought to a pH of  $7.0 \pm 0.5$  by addition of ammonium hydroxide.

Ultrasonic frequencies of 202, 358, 610, and 1060 kHz were generated using Allied Signal-Elac Nautik ultrasonic transducers with the reaction solution held in a 600 mL jacketed glass reactor. The applied power density was 250 W L $^{-1}$ . The calorimetric power density was determined to be  $75 \pm 10\%$  of the applied power density. The temperature was controlled at 10 °C with a Haake A80 refrigerated bath. All reactions were sparged with argon for at least 30 min prior to and during the reaction. PFBS and PFBA were sonicated simultaneously at initial concentrations of 0.30  $\mu\text{M}$  for PFBS and 0.47  $\mu\text{M}$  for PFBA. PFHS and PFHA were sonicated simultaneously at initial concentrations of 0.23  $\mu\text{M}$  for PFHS and 0.32  $\mu\text{M}$  for PFHA. Dilute concentrations (<1  $\mu\text{M}$ ) were chosen to maintain lightly populated bubble–water interfaces. The goal was to be in a concentration range where the barrier to adsorption was minimal and thus all observed kinetic effects could be attributed to sonochemistry. The specific concentrations were chosen because they were just below the highest concentration in the HPLC–MS calibration curve, thus yielding the widest analytical range possible. The variation in initial concentrations will not affect the results since they will be discussed in terms of pseudofirst order rate constants, which are normalized to the initial concentration.

PFC concentrations were analyzed by HPLC–ES–MS. The samples were placed into 750  $\mu\text{L}$  polypropylene autosampler vials and sealed with a PTFE septum crimp cap. Twenty microliters of collected or diluted sample was injected onto an Agilent 1100 LC for separation on a Betasil C18 column (Thermo-Electron) of dimensions 2.1 mm ID, 100 mm length, and 5  $\mu\text{m}$  particle size. A 2 mM aqueous ammonium acetate/methanol mobile phase at a flow rate of 0.3 mL min $^{-1}$  was used with an initial 5:95 aqueous/methanol composition. The eluent composition was increased to 90:10 over 12 min to separate the PFCs. HPLC effluents were analyzed with an Agilent ion trap mass spectrometer in the negative ion mode for the perfluorohexanesulfonate molecular ion ( $m/z = 399$ ), the perfluorobutanesulfonate molecular ion ( $m/z = 299$ ), the decarboxylated perfluorohexanoate ion ( $m/z = 269$ ), and the decarboxylated perfluorobutanoate ion ( $m/z = 169$ ). The nebulizer gas pressure was 40 PSI and the drying gas flow rate and temperature were 9 L min $^{-1}$  and 325 °C, respectively. The capillary voltage was set at +3500 V and the skimmer voltage was –15 V. Quantification was completed by first producing a calibration curve using 8 concentrations between 1 and 200 ppb fitted to a quadratic with  $X^{-1}$  weighting.

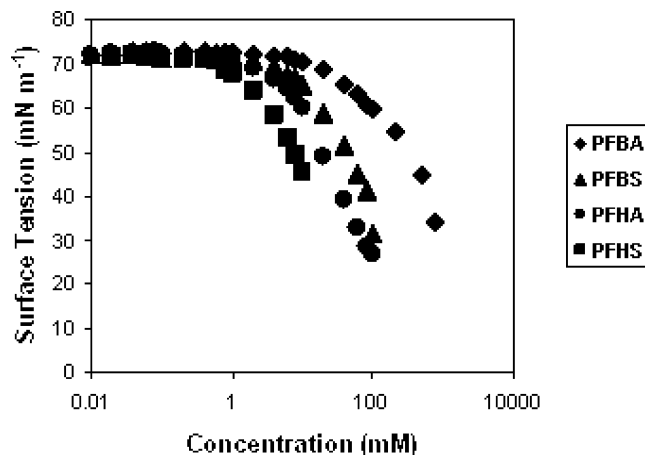


**Figure 1.** Plot of surface tension vs aqueous concentration of PFBS ( $\blacktriangle$ ), PFBA ( $\blacklozenge$ ), PFHS ( $\blacksquare$ ), and PFHA ( $\bullet$ ) (mM).

Surface tension measurements were made with a De Nouy tensiometer utilizing the ring method. The tensiometer was calibrated with a weight of known mass. Each sample was measured three times. The PFHS and PFBS surface tension measurements were on concentrations up to 10 and 100 mM, respectively, where the compounds became insoluble. The curve was fitted to the surface pressure equation of state using Matlab to determine the equilibrium air–water partitioning coefficient and the maximum surface concentration.

### Results and Discussion

**PFHX and PFBX Equilibrium Air–Water Interface Partitioning.** PFYX, where Y = H(exane) or B(utane) and X = c(A)rboxylate or S(ulfonate) equilibrium air–water partitioning coefficients were determined using concentration-dependent surface tension measurements. In Figure 1, the aqueous surface tension is plotted as a function of bulk PFYX concentration. From concentration-dependent surface tension measurements the maximum surface concentration,  $\Gamma_{\text{max}}^{\text{PFYX}}$  in mol/m $^2$ , and the bulk water to air–water partitioning coefficient,  $K_{\text{eq}}^{\text{PFYX}}$  in M $^{-1}$ , can be determined by fitting the data to the surface equation of state:

$$\Pi = \gamma_0 - \gamma_{[\text{PFYX}]} = nRT\Gamma_{\text{max}}^{\text{PFYX}} \ln(1 + K_{\text{eq}}^{\text{PFYX}}[\text{PFYX}]) \quad (1)$$

where  $\Pi$  is the surface pressure in N m $^{-1}$ ,  $\gamma_0 = 0.072$  N m $^{-1}$  is the surface tension of pure water, and  $\gamma_{[\text{PFYX}]}$  is the surface tension at the bulk aqueous FC concentration, [PFYX] in M, the gas constant,  $R = 8.314$  J K $^{-1}$  mol $^{-1}$ ,  $T = 295 \pm 1$  K, and  $n = 2$  for ionic surfactants. According to the surface tension results in Figure 1, the overall order of equilibrium surface partitioning is  $K_{\text{eq}}^{\text{PFHS}}(C_6) = 2.0K_{\text{eq}}^{\text{PFHA}}(C_5) = 3.9K_{\text{eq}}^{\text{PFBS}}(C_4) = 5.0K_{\text{eq}}^{\text{PFBA}}(C_3)$ .  $C_n$  represents the number of carbons in the hydrophobic, fluorocarbon tail.

Of note in Figure 1 is the fact that the sulfonates, including PFOS, all become insoluble prior to reaching their critical micelle concentration (i.e., when maximum adsorption is attained). The perfluoro-sulfonate insolubility occurs at a surface tension of  $40 \pm 5$  mN m $^{-1}$ , suggesting there is a critical surface pressure at which perfluoroalkanesulfonates reach their solubility limit.

Listed in Table 2 are the maximum surface concentrations,  $\Gamma_{\text{max}}^{\text{PFYX}}$  in mol m $^{-2}$ , equilibrium partitioning constants,  $K_{\text{eq}}^{\text{PFYX}}$  in M $^{-1}$ ,  $C_{\text{max}}$  in M calculated by setting  $\theta = 0.9$  in eq 3 (a surrogate



**TABLE 2: Equilibrium PFC Air–Water Interface Partitioning Constants**

PFC	$K_{eq}$ (L mol <sup>-1</sup> )	$\Gamma_{max}$ (mol m <sup>-2</sup> )	$C_{max}^a$ (mM)	$R^2$
PFOS	1871 ± 852 <sup>b</sup>	$(5.0 \pm 2.2) \times 10^{-6}$	4.8	0.99
PFHS	158 ± 32.8	$(5.7 \pm 0.8) \times 10^{-6}$	57	0.999
PFBS	40.4 ± 8.60	$(4.4 \pm 0.5) \times 10^{-6}$	223	0.998
PFOA	361 ± 25.3 <sup>b</sup>	$(4.4 \pm 0.2) \times 10^{-6}$	24.9	
PFHA	75.6 ± 11.4	$(4.8 \pm 0.4) \times 10^{-6}$	119	0.998
PFBA	31.7 ± 4.8	$(1.95 \pm 0.12) \times 10^{-6}$	284	0.998

<sup>a</sup>  $C_{max}$  is calculated by setting  $\theta = 0.9$  in eq 3. <sup>b</sup>  $\Gamma_{max}$  and  $K_{eq}$  values for PFOS and PFOA are listed for comparison.<sup>32</sup>

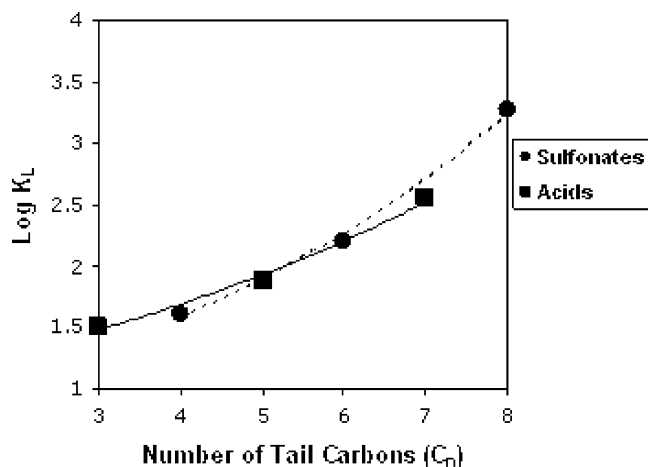


**Figure 2.** Plot of the air–water interface partitioning coefficient as a function of fluorochemical chain length for the sulfonates (●) and carboxylates (■).  $K_{eq}$  values<sup>32</sup> for  $C_8$  surfactants are plotted for comparison.

for the CMC since some species become insoluble prior)<sup>55</sup> and the  $R^2$  of fitting to eq 1 for PFBX, PFHX, and PFOX, from previous results.<sup>32</sup> With the exception of PFBA,  $\Gamma_{max}^{PFYX}$  is similar for all the compounds. In Figure 2,  $K_{eq}^{PFYX}$  is plotted as a semilog function of the  $C_n$ -tail. Overall, there is a wide range of  $K_{eq}^{PFYX}$  that spans 2 orders of magnitude for the perfluoro-carboxylates and -sulfonates. Note that the perfluoro-carboxylates have one less  $-CF_2-$  than the perfluoro-sulfonates even though they have an equivalent number of carbons (e.g., PFOA =  $C_7$ -tail and PFOS =  $C_8$ -tail). The semilog perfluoro-carboxylate and -sulfonate empirically fit to the equations:  $\log K_{eq,sulfonates} = 0.78e^{0.18C_n}$ ;  $\log K_{eq,carboxylates} = 0.99e^{0.13C_n}$ . The empirical fits are at variance with hydrocarbon results, which generally yield a linear dependence. The perfluoro-carboxylate and -sulfonate curves in Figure 2 do not overlap, indicating the headgroup speciation affects the air–water interface partitioning, with the perfluoro-carboxylate being less surface active than the perfluoro-sulfonate. This result is in qualitative agreement with previously reported acetic acid<sup>34</sup> and methanesulfonate<sup>35</sup> hydration energies. The greater hydration free energy of acetic acid as compared to methanesulfonate indicates that it will associate itself to a greater extent with bulk water implying a lower interfacial activity.

The calculated  $\Gamma_{max}^{PFYX}$  values all fall into the range  $(5.0 \pm 0.7) \times 10^{-6}$  mol m<sup>-2</sup> except for PFBA, which has a maximum surface concentration,  $\Gamma_{max}^{PFBA} = (1.95 \pm 0.1) \times 10^{-6}$  mol m<sup>-2</sup>. The maximum surface concentration is a balance between attractive forces of the hydrophobic tail to the air–water interface and steric/Coulombic repulsion of neighboring hydrophilic headgroups.<sup>36</sup> Neutron reflectivity studies have estimated that the first 2–3 PFOA carbons are below the air–water interface.<sup>37</sup> Assuming a similar structure for PFBA, > 50% of

its carbons would be beneath the air–water interface. The reduction in hydrophobic tail interactions for PFBA can be semiquantitatively evaluated by conversion of maximum surface concentrations to area per molecule which would be 0.6 nm<sup>2</sup>/PFYX and 1.5 nm<sup>2</sup>/PFBA, which converts to a circle of radius  $r = 0.16$  nm and  $r = 0.26$  nm, respectively. 0.16 nm is on the order of the C–F bond length (0.13 nm) in CHF<sub>3</sub>, suggesting relatively intimate contact between hydrophobic chains, whereas the 0.26 nm in PFBA is more representative of an ionic hydration sphere (0.3–0.4 nm), suggesting that the hydrophobicity of PFBA's short tail ( $C_3$ ) cannot compensate for the Coulombic repulsion between neighboring carboxylate groups.

**PFHX and PFBX Frequency-Dependent Sonochemical Kinetics.** The semilog time-dependent sonochemical degradation profiles of aqueous PFHS, PFHA, PFBS, and PFBA at acoustic frequencies of 202, 358, 610, and 1060 kHz ( $PD = 250$  W L<sup>-1</sup>,  $T = 10$  °C, Ar) are depicted in Figure 3a–d, respectively. Each data point represents the average of three experiments (error bars were not added due to space considerations). Ultrasonic irradiation was performed at initial PFC concentrations of  $[PFBA]_i = 0.47$   $\mu$ M,  $[PFBS]_i = 0.30$   $\mu$ M,  $[PFHA]_i = 0.32$   $\mu$ M, and  $[PFHS]_i = 0.23$   $\mu$ M at an initial pH of  $7.0 \pm 0.5$ . The initial PFC concentrations were degraded by at least PFBA (57%), PFBS (66%), PFHS (86%), and PFHA (90%) after 120 min of exposure to ultrasound at all frequencies. In comparison, PFOS and PFOA, were degraded to 87% and 99% of their initial concentrations after 120 min of ultrasonic irradiation.

The plots of  $\ln [PFYX]_f/[PFYX]_i$  (where Y signifies the chain length B (butane), H (hexane), O (octane), and X signifies the headgroup A (carboxylate) or S (sulfonate)) vs time plots are linear indicating pseudo-first-order kinetics, Figure 3a–d, consistent with an interfacial pyrolysis decomposition mechanism where PFYX concentrations are well below maximum bubble surface adsorption levels (e.g., the submicromolar PFYX concentrations are significantly below the concentration where surface tension begins to decrease). Thus, the sonochemical degradation rate of PFYX can be expressed by eq 2:

$$d[PFYX]/dt = -k_{app}^{PFYX}[PFYX] \quad (2)$$

$k_{app}^{PFYX}$  is the apparent first-order rate constant and  $[PFYX]$  the bulk concentration. When PFYX decreases below 10 nM, the plots of  $\ln [PFYX]_f/[PFYX]_i$  are no longer linear, suggesting a change in kinetic order. This result requires further investigation, and the data will not be used for this study. Rate constants determined from linear regression of data in Figure 3 at 358 kHz and the PFOX data from other studies follows the order:  $k_{app,358}^{PFOA} \approx k_{app,358}^{PFHA} \approx 1.3k_{app,358}^{PFOS} \approx 1.3k_{app,358}^{PFHS} \approx 2.2k_{app,358}^{PFBS} \approx 3.3k_{app,358}^{PFBA}$ . The pseudo-first-order rate constants and half-lives for the degradation of the six perfluoro-compounds at 250 W L<sup>-1</sup> and 358 kHz are listed in Table 3. PFHX relative rates are similar to relative rates observed for the PFOX where  $(k_{app}^{PFOA})/(k_{app}^{PFOS}) = 1.7$  and  $(k_{app}^{PFHA})/(k_{app}^{PFHS}) = 1.8$ , reflecting that the carboxylates degrade faster than the sulfonates. In agreement with previous results,<sup>16,17,32,33</sup> the perfluoro-carboxylate degradation rates for PFOA and PFHA are faster than their respective perfluoro-sulfonate degradation rates for PFOS and PFHS. And the PFHA rate is faster than the PFOS rate. This is attributed to the perfluoro-carboxylates having lower thermal activation energies than perfluoro-sulfonates and thus a higher intrinsic chemical reaction rate (i.e., interfacial high-temperature sonolysis). In contrast, the degradation rate constant for the  $C_4$  sulfonate is 1.5 times that of the carboxylate,  $(k_{app}^{PFBA})/(k_{app}^{PFBS}) = 0.66$ ,

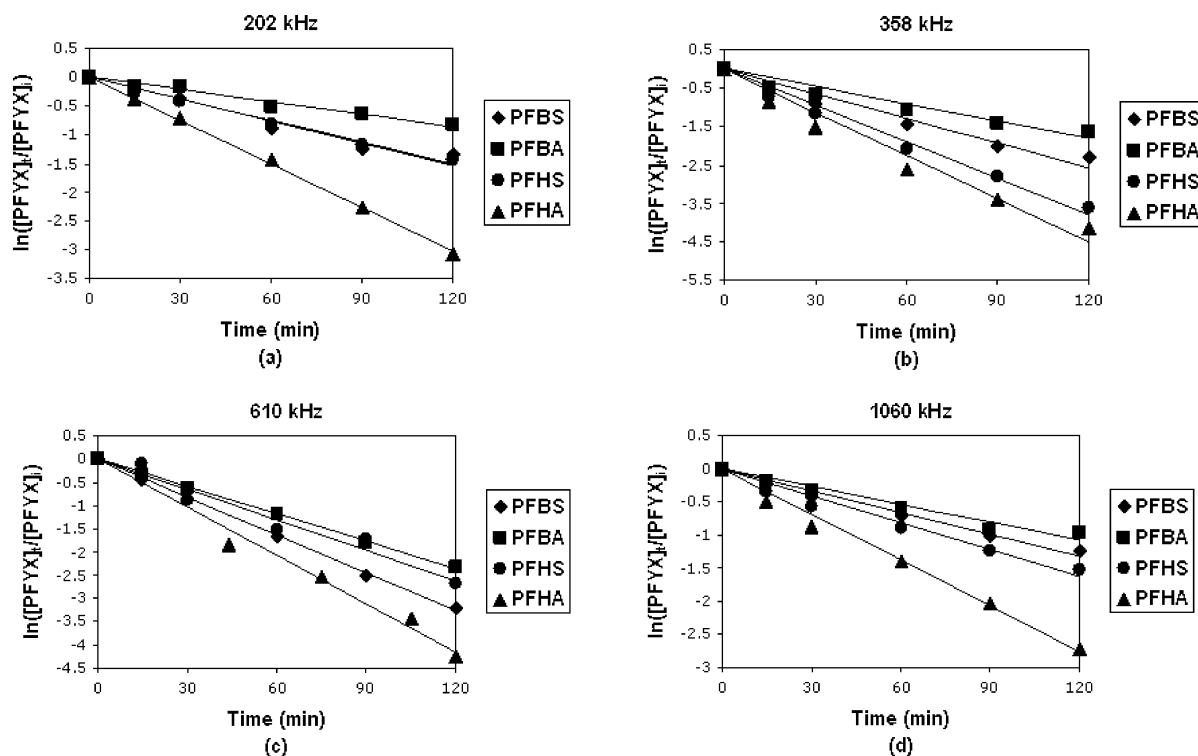


**Figure 3.** Time-dependent degradation of PFYX at 250 W L<sup>-1</sup> in Ar(g) saturated solutions at pH 7 and 10 °C: PFHA (▲), PFHS (●), PFBA (■), and PFBS (◆). (a) 202 kHz,  $k_{\text{app}}^{\text{-PFBS}} = 0.013$ ;  $k_{\text{app}}^{\text{-PFBA}} = 0.007$ ;  $k_{\text{app}}^{\text{-PFHS}} = 0.012$ ;  $k_{\text{app}}^{\text{-PFHA}} = 0.019$ . (b) 358 kHz,  $k_{\text{app}}^{\text{-PFBS}} = 0.018$ ;  $k_{\text{app}}^{\text{-PFBA}} = 0.012$ ;  $k_{\text{app}}^{\text{-PFHS}} = 0.030$ ;  $k_{\text{app}}^{\text{-PFHA}} = 0.039$ . (c)  $k_{\text{app}}^{\text{-PFBS}} = 0.023$ ;  $k_{\text{app}}^{\text{-PFBA}} = 0.017$ ;  $k_{\text{app}}^{\text{-PFHS}} = 0.022$ ;  $k_{\text{app}}^{\text{-PFHA}} = 0.036$ . (d)  $k_{\text{app}}^{\text{-PFBS}} = 0.009$ ;  $k_{\text{app}}^{\text{-PFBA}} = 0.008$ ;  $k_{\text{app}}^{\text{-PFHS}} = 0.012$ ;  $k_{\text{app}}^{\text{-PFHA}} = 0.022$ . The  $k$ 's are in min<sup>-1</sup>.

**TABLE 3: PFC Sonochemical Rate Constants and Half-Lives for the Degradation of PFYX, Where Y = B, H, or O and X = A or S under Ultrasonic Conditions: 358 kHz, 250 W L<sup>-1</sup>, 10 °C, Ar**

PFC	$k_{\text{app}}$ (min <sup>-1</sup> )	$\tau_{1/2}$ (min)
PFBA	0.012 ± 0.001	57.2
PFBS	0.018 ± 0.002	42.3
PFHA	0.053 ± 0.001	16.8
PFHS	0.030 ± 0.003	23.2
PFOA <sup>a</sup>	0.048 ± 0.001	16.9
PFOS <sup>a</sup>	0.028 ± 0.005	25.7

<sup>a</sup>  $k_{\text{app}}$  values of PFOS and PFOA listed for comparison.<sup>17</sup>

suggesting a change in bubble–water interface adsorption for the shorter-chain since chain-length effects on the thermal activation energy is expected to be minimal.

The PFBX and PFHX sonochemical degradation rate constants,  $k_{\text{app}}^{\text{PFYX}}$ , were determined in this work at acoustic frequencies ranging from 202 to 1060 kHz at an applied acoustic power density of 250 W L<sup>-1</sup>, at 10 °C in argon. The PFOX rates were taken from Vecitis et al.<sup>17</sup> The pseudo-first-order sonolytic rate constants,  $k_{\text{app}}^{\text{PFYX}}$ , versus frequency for PFBA, PFBS, PFHA, PFHS, PFOA, and PFOS are plotted in Figure 4a,b, for the sulfonates and carboxylates, respectively. The degradation rate constants for the PFHX and PFOX have apparent maxima at 358 kHz. The PFBX sonochemical degradation rate constants have apparent maxima at 610 kHz, again suggesting a change in bubble interface adsorption for these shorter chain length FC surfactants. The observed PFOX and PFHX rate constant vs frequency trends are comparable with previous reports<sup>38</sup> on the sonochemical degradation of chlorocarbons. Rate maxima at 358 kHz are due to maximum number of bubble events per unit time. The observed PFBX kinetically optimal frequency of 610 kHz is similar to reports on chlorocarbon sonolysis.<sup>24,39</sup> A

sonolytic rate maximum at 610 kHz is due to enhanced bulk aqueous to cavitating bubble mass transfer effects.<sup>24</sup>

**Sonochemical Kinetics Frequency Dependence.** Acoustic frequency is one of many sonochemical parameters that modulate the cavitation dynamics of the bubble cloud present in solution. Sonochemical parameters such as power density,<sup>25,40,41</sup> reactor design,<sup>25</sup> area of the emitting surface,<sup>41</sup> dissolved gas,<sup>40</sup> and nature of the solvent,<sup>40</sup> also affect cavitation dynamics. Variations on the applied frequency can affect (1) the average temperature and pressure inside a transiently cavitating bubble,<sup>19,27,40,42</sup> (2) the number and reactor volumetric distribution of cavitating bubbles,<sup>40</sup> (3) bubble radius and “hot spot” lifetime<sup>18,26,40,43,44</sup> (4) the dynamics and symmetry of collapse,<sup>26,40,43,44</sup> and (5) radical dispersion into solution.<sup>40,41,45</sup> All the previously stated factors are interdependent in controlling sonochemical events.

The effect of acoustic frequency on sonochemical kinetics has been previously reported for a number of chemicals.<sup>18,19,39–46</sup> The rate of sonochemical potassium iodide oxidation was increased 8-fold at 300 kHz compared to 20 kHz at 2 W of applied power.<sup>41</sup> The first-order rate constant for the degradation of aqueous phenyl trifluoromethylketone was 14 times higher at 515 kHz as compared to 30 kHz.<sup>19</sup> The maximum 1,4-dioxane sonochemical reaction rates was observed at 358 kHz over the frequency range 205–1071 kHz.<sup>44</sup> Over the range 20–1000 kHz, the highest rate of H<sub>2</sub>O<sub>2</sub> and hydroxyl radical production was observed at 500 kHz during sonolysis and the lowest production rates occurred at 20 kHz, and the relative rates were not affected by the sparging gas.<sup>26</sup> Finally, the first-order degradation rate constants for chlorinated methanes, ethanes, and ethenes sonicated over the frequency range 205–1078 kHz showed an apparent maximum at 618 kHz.<sup>39</sup>

Sonochemical kinetic frequency dependences are due to multiple effects. Average bubble vapor temperatures have little

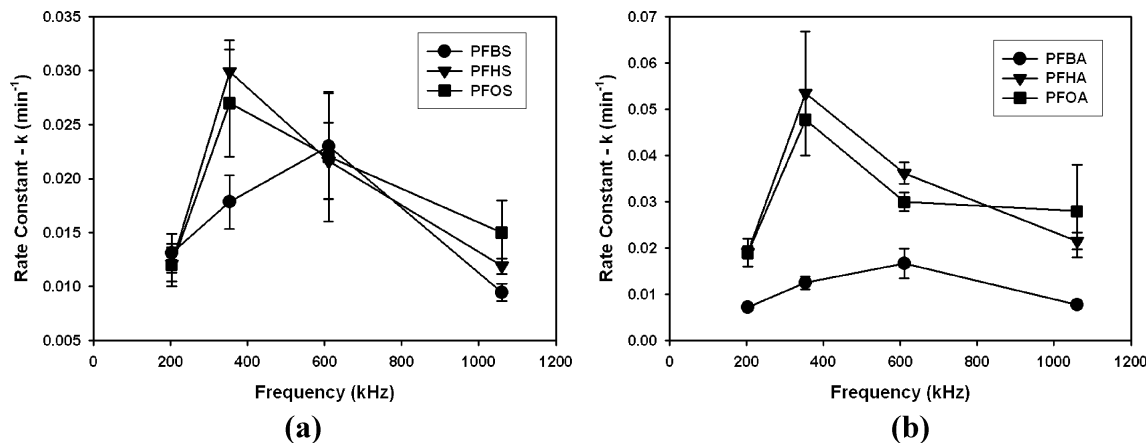


**Figure 4.** Pseudo-first-order rate constant as a function of frequency. Ultrasound conditions:  $f = 202, 358, 610,$  and  $1060$  kHz at  $250 \text{ W L}^{-1}$ ,  $10^\circ\text{C}$ , Ar for (a) PFBS (●), PFHS (▼), and PFOS (■) and (b) PFBA (●), PFHA (▼), and PFOA (■).  $k^{-\text{PFOX}}$  values<sup>17</sup> are plotted for comparison.

**TABLE 4: Theoretical Resonance Radius Values ( $\mu\text{m}$ ) and Collapse Times ( $\mu\text{s}$ ) as a Function of Frequency (kHz)**

frequency (kHz)	resonant radius ( $\mu\text{m}$ )	surface area $A$ ( $\mu\text{m}^2$ )	volume $V$ (nL)	$A/V$ ( $\mu\text{m}^{-1}$ )
202	17.8	$3.97 \times 10^3$	0.023	0.17
358	10.0	$1.26 \times 10^3$	0.0042	0.30
610	5.88	$4.34 \times 10^2$	0.00085	0.51
1060	3.38	$1.43 \times 10^2$	0.00016	0.88

frequency dependence,<sup>42</sup> suggesting that the total number of bubble events per unit time is a primary factor in determining sonochemical kinetics. At higher frequencies,  $>100$  kHz, the total number of transient cavitation bubble events per unit time is larger and the active bubble populations accounts for a larger fraction of the total reactor volume.<sup>19,47</sup> Thus, if all cavitation events result in similar vapor and interfacial temperatures, the frequency with the greatest transient events per unit time would also be expected to maximize sonolytic rates. Enhanced mass transfer brought on by high-velocity bubble oscillations will also increase the PFC diffusion rate from bulk water to the bubble interface.<sup>29,32,39,48</sup> As acoustic frequency increases, a stable cavitation bubble will oscillate more frequently per unit time leading to a more rapid rectified diffusion.

A rough estimation of the enhanced mass transfer dependence on frequency will be made. The theoretical resonance radius of a bubble is given by the equation  $R_r^2 = 3\kappa P_0/\rho\omega_r^2$ , where  $R_r$  represents the resonance radius,  $\omega_r$  the resonance frequency,  $\rho$  the density of the solution,  $\kappa$ , the polytropic index, and  $P_0$ , the hydrostatic pressure.<sup>24,26</sup> For example, in Table 4 the theoretical resonance radius of bubbles produced at frequencies of 202.6, 358, 610, and 1060 kHz are listed, reflecting the changes between the relative interfacial properties versus the gas-phase properties. Comparisons between bubble surface sites to gas-phase sites as a function of frequency reveals that smaller cavitation bubbles with larger surface to volume ratios become prominent at higher frequencies.<sup>24</sup> Thus, increasing frequency results in more bubble events per unit time and more extensive mass transfer of the solute from the bulk to the bubble interface<sup>24</sup> due to an increase in surface active sites for enhanced adsorption. As a result, at higher frequencies there is enhanced mass transport of weakly partitioning PFCs from the bulk solution to the cavitation bubble interface, where they can be decomposed by interfacial pyrolysis.

The total number of active bubble events per unit time and the mass transfer of the perfluorinated species to the bubble surface<sup>44</sup> are two frequency-dependent factors that act concomitantly on PFC degradation kinetics. The apparent frequency

maximum for PFHX is 358 kHz and for PFBX is 610 kHz (Figure 4a,b). Since 358 kHz is the optimal frequency for PFHX sonochemical kinetics, it suggests that the number of cavitation events per unit time and thus the intrinsic maximum chemical reaction rate mediates PFHX degradation kinetics. As 610 kHz is the optimal frequency for PFBX sonolysis, it suggests that mass transfer to the bubble–water interface and thus extent of adsorption is rate limiting. Consistent with surface tension results, Figure 1 and Table 2, which indicate that PFBX is less surface active than PFHX.<sup>28,30,49</sup>

For PFHX and PFBX, as the frequency increases beyond its optimal value, 358 and 618 kHz, respectively, decomposition rates decrease approximately linearly with increasing frequency. At the highest frequency tested, 1060 kHz, the half-period for rarefaction of the acoustic wave is only  $0.47 \mu\text{s}$ , which is insufficient time for the bubble to undergo the rapid growth required for transient cavitation, limiting the number of transient cavitation events per unit time. The  $0.47 \mu\text{s}$  compression half-period is approaching the characteristic time for transient bubble collapse and may interrupt these high-temperature events prior to completion. The gas and interface temperatures of these stable cavitation bubbles are greater than ambient but do not approach the extremes of transiently cavitating bubbles.<sup>21</sup> Furthermore, the time available during bubble oscillations is too short compared to the length of time necessary for the surfactants to achieve equilibrium adsorption to the bubble–water interface.<sup>30</sup> The lower number of transient bubble events per unit time and adsorption limitations with increasing frequency results in a decrease in PFC sonochemical rates (Figure 4a,b).

**PFHX and PFBX Sonochemical Kinetics Adsorption Dependence.** Ultrasonic irradiation of aqueous solutions creates three distinct reaction zones of varied intensity proportional to their proximity to the bubble core: (1) the core of the bubble vapor “hot spot”, (2) the gas and water shell surrounding the hot core, and (3) the bulk solution at near ambient temperature.<sup>30</sup> The extreme temperatures (ca. 4000 K) and pressures of the bubble core (1) yields high radical densities. A fraction of these radicals will diffuse to the bubble–water interface (2) prior to recombination. An even lesser fraction of radicals will make it to the bulk water (3) via bubble jets and eddy diffusion.

The physicochemical properties of a compound will determine its relative partitioning into each of the three acoustic cavitation zones, which in turn will be proportional to that compounds sonochemical kinetics. For example, the relatively high Henry’s law constants for carbon tetrachloride and chloroform ( $K_H = 2454 \text{ Pa m}^3 \text{ mol}^{-1}$  for  $\text{CCl}_4$  and  $537 \text{ Pa m}^3 \text{ mol}^{-1}$  for  $\text{CHCl}_3$ ),<sup>39,50</sup>



corresponds to their preferred localization at the high-temperature bubble interior (205 kHz, 0.15 mM,  $k = 7.3 \times 10 \text{ s}^{-1}$  for  $\text{CCl}_4$  and  $4.7 \times 10 \text{ s}^{-1}$  for  $\text{CHCl}_3$ ).<sup>39</sup> The sonolysis products of aqueous solutions containing surfactants OGP (*n*-octyl- $\beta$ -D-glucopyranoside) and DGP (*n*-decyl- $\beta$ -D-glucopyranoside) indicated surfactant localization at the bubble–water interface (0.1–6 mM, 614 kHz or 1.057 MHz).<sup>51</sup> In this case, the surfactants reacted with OH radicals that had diffused from the bubble core to the surface, which lead to an apparent, strong inhibition of  $\text{H}_2\text{O}_2$  production.

Concentration-dependent sonochemical kinetics of PFOA and PFOS were well fit to the Langmuir–Hinshelwood model,<sup>32</sup> where kinetic saturation is a result of a finite number of adsorption sites. The experiments performed here were at dilute surfactant ( $>1 \mu\text{M}$ ), orders of magnitude below bubble interface saturation. The sonochemical kinetics observed here can be modeled as the low-concentration limit of Langmuir–Hinshelwood kinetics.<sup>52</sup> The observed rate is proportional to  $\theta^{\text{PFYX}}$ , a fraction of the maximum bubble–water interface binding sites occupied by PFYX molecules, eq 3<sup>32</sup> and the absolute degradation rate can be modeled by eq 4.

$$\theta^{\text{PFYX}} = \frac{K_{\text{eq}}^{\text{PFYX}}[\text{PFYX}]}{1 + K_{\text{eq}}^{\text{PFYX}}[\text{PFYX}]} \quad (3)$$

$$\frac{d[\text{PFYX}]}{dt} = -k_{\text{app}}^{\text{PFYX}}[\text{PFYX}] = -k_{\Delta}^{\text{PFYX}}\theta^{\text{PFYX}} \quad (4)$$

$k_{\text{app}}^{\text{PFYX}}$  is the pseudo-first-order rate constant in  $\text{s}^{-1}$  and  $k_{\Delta}$  is the maximum intrinsic chemical reaction rate in  $\text{M s}^{-1}$  attained when all the transiently cavitating bubble surface sites are occupied. At low concentrations, eq 5, when the bubble surface is lightly populated, eq 3 can be reduced to eq 6 and eq 4 can be reduced to eq 7.

$$K_{\text{eq}}^{\text{PFYX}}[\text{PFYX}] \ll 1 \quad (5)$$

$$\theta^{\text{PFYX}} = K_{\text{eq}}^{\text{PFYX}}[\text{PFYX}] \quad (6)$$

$$\frac{d[\text{PFYX}]}{dt} = -k_{\Delta}^{\text{PFYX}}K_{\text{eq}}^{\text{PFYX}}[\text{PFYX}] \quad (7)$$

$$k_{\text{app}}^{\text{PFYX}} = k_{\Delta}^{\text{PFYX}}K_{\text{eq}}^{\text{PFYX}} \quad (8)$$

In the low-concentration regime of the Langmuir–Hinshelwood model, the kinetics are mediated by the fraction of the total PF molecules adsorbed to the bubble–water interface yielding apparent first-order kinetics.<sup>32</sup>

According to the equilibrium partitioning coefficients listed in Table 2 and Figure 2 where the  $K$ 's are plotted as a function of the tail carbon number, the partitioning coefficient is roughly correlated with  $C_n$  and the sulfonates adsorb to the air–water interface more effectively than acids.<sup>32</sup> However, the perfluorocarboxylate sonochemical kinetics are faster than the perfluorosulfonates for the  $C_6$  and  $C_8$  compounds, indicating a larger PF-sulfonate thermal activation energy, in agreement with previous reports.<sup>17,53</sup> Also, the  $C_6$  and  $C_8$  sulfonates have similar degradation rates,  $k_{\text{app}}^{\text{PFOS}} \approx k_{\text{app}}^{\text{PFHS}}$ , and the  $C_6$  and  $C_8$  carboxylates have similar degradation rates,  $k_{\text{app}}^{\text{PFOA}} \approx k_{\text{app}}^{\text{PFHA}}$ , suggesting for  $C_6$  and  $C_8$  surfactants under dilute concentrations, adsorption

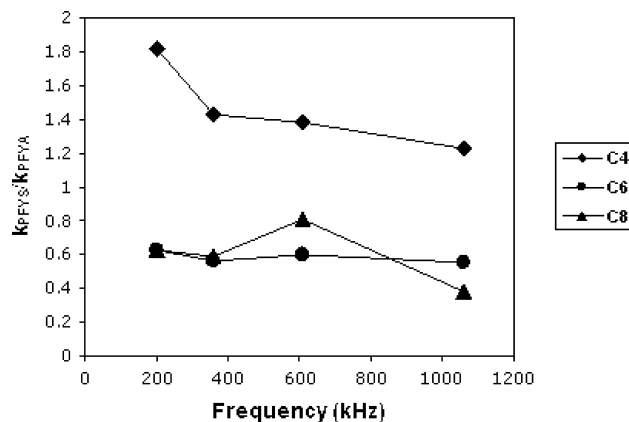


**Figure 5.** Frequency effects on the ratio of sonochemical degradation rate constants,  $k(\text{sulfonate})/k(\text{carboxylate})$ . PFBX- $C_4$  (◆), PFHX- $C_6$  (●), and PFOX- $C_8$  (▲), where X = A or S. Values of  $k^{\text{PFOX}}$  obtained from Vecitis et al.<sup>17</sup>

is mediated by high-velocity radial oscillations and not equilibrium partitioning processes. In contrast, the  $C_4$  PF-sulfonates degrade faster than the PF-carboxylates and the PFBX degradation rates are slower than their PFOX and PFHX analogs,  $k_{\text{app}}^{\text{PFOX}} \approx k_{\text{app}}^{\text{PFHX}} > k_{\text{app}}^{\text{PFBX}}$ , with the relative difference being greater for the shorter  $C_3$ -tail, PFBA,  $k_{\text{app}}^{\text{PFHA/PFOA}}/k_{\text{app}}^{\text{PFBA}} = 4.4$ , than for the  $C_4$ -tail, PFBS,  $k_{\text{app}}^{\text{PFHS/PFOS}}/k_{\text{app}}^{\text{PFBS}} = 1.6$ . Suggesting that once the perfluorinated tail length is less than 5 carbons ( $C_4$ -PFBS,  $C_3$ -PFBA), the dynamic, FC adsorption to the bubble interface occurs to a lower extent. As the tail length decreases, the hydrophobic interfacial attraction cannot compensate for the Coulombic repulsion between the ionic headgroups.<sup>36</sup> On the contrary, PFBS and more so PFBA are relatively more water-soluble as a result of their shorter hydrophobic chain length, consistent with PFBA's smaller maximum surface excess concentration.

Figure 5 shows the ratio of sonochemical degradation rate constants,  $k(\text{sulfonate})/k(\text{carboxylate})$  as a function of frequency for the three carbon numbers. At 358 kHz, the ratio of PFBS to PFBA rate constants is  $>1$  whereas the  $C_6$  and  $C_8$  ratios are  $<1$ ,  $k_{\text{app}}^{\text{PFBS}} = 1.5k_{\text{app}}^{\text{PFBA}}$  vs  $k_{\text{app}}^{\text{PFHA/PFOA}} = 1.7\text{--}1.8k_{\text{app}}^{\text{PFHS/PFOS}}$ . This holds true at all frequencies, once again suggesting a change in dynamic, for ultrasonically driven adsorption for PFCs with  $C_n$ -tail  $< 5$ . For PFHX and PFOX, frequency has little effect on the ratio of rate constants. For PFBX, the ratio is observed to decrease with increasing frequency. PFBS is the stronger surfactant (reduction of surface tension by  $2 \text{ mN m}^{-1}$  occurs at 2 mM for PFBS versus 10 mM for PFBA) yet PFBA rates increased to a greater extent with increasing frequency, indicating ultrasonic effects on dynamic adsorption to the bubble interface.

The ultrasonic effects on PFC bubble–water interface adsorption kinetics could be a result of high-velocity radial oscillations enhancing PFC diffusion to the bubble. The time scale of bubble growth is short (microseconds) compared to the time required for the surfactants to equilibrate with the gas solution interface of the bubble (milliseconds), which would imply lower than equilibrium adsorption.<sup>30</sup> For example, at 47 kHz, a 2 mM aqueous sodium dodecyl sulfate (SDS), an anionic hydrocarbon surfactant, solution reached equilibrium with the air–water interface after  $>3 \text{ m}$ , which is much longer than the acoustic cycle of  $20 \mu\text{s}$ .<sup>30,54</sup> However, at  $f > 10 \text{ kHz}$ , bubble radial oscillation velocities are much faster than chemical diffusion rates,  $v_{\text{bub,rad}} \gg v_{\text{diffusion}}$ .<sup>48</sup> And once adsorbed to the air–water interface, strong surfactants such as SDS (CMC =



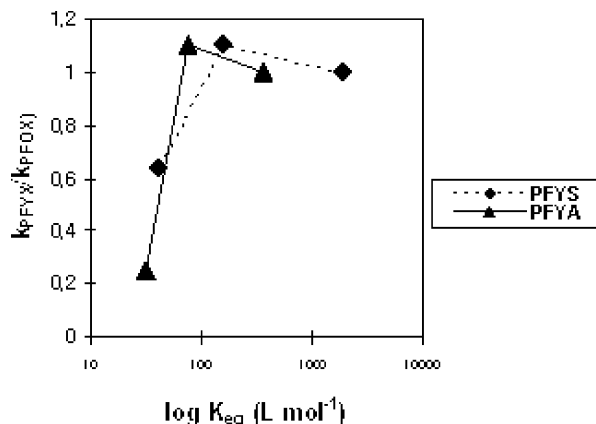


**Figure 6.** Apparent rate constants normalized to the PFOX rate constant vs equilibrium partitioning coefficients,  $K_{eq}^{PFYX}$ .  $K_{eq}$  and  $k^{PFOX}$  values obtained from Vecitis et al.<sup>17,32</sup>

8.0 mM) have negligible diffusion rates away from the interface,  $k_{desorb} = 500 s^{-1}$  or  $\tau_{1/2} > 1 ms$ ,<sup>55</sup> which is much longer than estimated bubble lifetimes 10–100  $\mu s$ . Thus, once adsorbed to a cavitating bubble, strong surfactants such as SDS (PFOA has similar surfactant properties) are not expected to desorb over the bubble lifetime. Due to the large volume covered by the radial bubble oscillations, irreversible interfacial adsorption gives little room for mass transfer enhancements.

However, if a species was able to diffuse away from the bubble–water interface over a relevant time scale,  $(\ln 2)/k_{desorb} < 100 \mu s$ , and mass transfer was enhanced during sonochemistry,  $k_{adsorb} = k_{bub,osc}$ , mass transfer enhancements with increasing frequency can be rationalized. If the perfluorochemical were able to desorb during a nontransient, bubble compression phase, they could be readsorbed during the subsequent rarefaction phase.  $K_{eq} = k_{adsorb}/k_{desorb}$ , and if  $k_{adsorb}$  but not  $k_{desorb}$  is ultrasonically enhanced, then an increase in  $K_{eq}$  would be expected.  $k_{adsorb}$  will increase with increasing frequency due to increased SA/V ratios and increased frequency of bubble oscillations per unit time. Sonochemical frequency dependences, Figure 5, suggest this is active for the perfluorinated species with  $C_n$ -tail  $< 5$  or  $K_{eq} < 50 M^{-1}$ . Consistent with previous arguments, see Adsorption section, that PFBA is not hydrophobic enough to counteract Coulombic repulsions of the headgroups and thus has a lower maximum surface concentration.

The apparent rate constants normalized to the PFOX rate constant,  $k_{app}^{PFYS}/k_{app}^{PFOX}$  or  $k_{app}^{PFYA}/k_{app}^{PFOX}$  vs the equilibrium partitioning values,  $K_{eq}^{PFYX}$ , for  $f = 358 kHz$  are plotted in Figure 6. The rate constants are normalized to the  $C_8$  rate constant to cancel any headgroup effects on kinetics. Assuming that PFC chain length has minimal effect on the thermal activation energy and thus intrinsic chemical reaction rate,  $k_A^{PFYX}$  in eq 7, differences in sonochemical kinetics should be solely due to extent of adsorption to the bubble water interface,  $K_{eq}^{PFYX}$  in eq 7, which is correlated with hydrophobic tail length, Figure 2. However, in Figure 6, there is no correlation between the equilibrium partitioning constant and the  $C_8$ -normalized sonochemical degradation rate constant. When  $C_n$ -tail  $> 5$  or  $K_{eq}^{PFYX} \gg 50 M^{-1}$ , the fluorocarbon hydrophobic tail length has no effect on the normalized rate constants  $(k_{app}^{PFYX})/(k_{app}^{PFOX}) = 1.0 \pm 0.1$ . This suggests that above a threshold partitioning constant value, bubble–water interface adsorption is ultrasonically mediated. This would correspond to a  $k_{desorb}$  value being too low for surfactant desorption to occur over the bubble lifetime.

The equivalent normalized rate constants for  $C_n$ -tail  $> 5$  suggest that under lightly populated bubble–water interface

conditions, adsorption is ultrasonically mediated and can not be described by equilibrium air–water interface partitioning coefficients. In agreement with Langmuir–Hinshelwood modeling<sup>32</sup> of concentration-dependent PFOS and PFOA kinetics that indicated ultrasonic enhancement of PFOX adsorption to the bubble–water interface under dilute conditions. There is an apparent hydrophobic tail length threshold for the observed ultrasonic adsorption effects as seen in the decreasing normalized rate constants for  $C_n$ -tail  $< 5$  and  $K_{eq} < 50 M^{-1}$ . The greater water solubility of the PFCs with shorter tails results in an inability of the shorter PFCs to form stable surface films, and thus they are able to desorb for the interface within the transiently cavitating bubble lifetime.

## Conclusions

The sonochemical degradation kinetics of perfluoroalkancarboxylates and -sulfonates is influenced by their adsorption behavior at the air–water interface and the applied acoustic frequency. Equilibrium partitioning coefficients,  $K_{eq}^{PFYX}$ , of perfluoroalkancarboxylates and -sulfonates increase with increasing hydrophobic chain length,  $C_n$ . Equilibrium bubble surface partitioning coefficients,  $K_{eq}^{PFYX}$ , were shown to have no correlation to PFHX and PFOX ( $C_{n \geq 4}$ ) sonochemical kinetics,  $k_{app,f}^{PFYX}$ . For PFHX and PFOX, adsorption is ultrasonically mediated under lightly populated conditions. Initial results suggest a possible correlation between  $K_{eq}^{PFYX}$  and  $k_{app,f}^{PFYX}$  for PFBS ( $C_4$ ) and PFBA ( $C_3$ ), which have the shortest perfluorinated, hydrophobic chain length and are least surface active. PFHX and PFOX exhibit sonolytic rate maxima at 358 kHz, and PFBX exhibits rate maxima at 610 kHz. These results suggest that the number of cavitation events per unit time (PFOX/PFBX) and enhanced mass transfer to the bubble–water interface (PFBX) to be the respective sonochemical degradation rate mediators. Dilute aqueous perfluorinated surfactant sonochemical degradation rates are a complex function of both physiochemical properties such as air–water interface partitioning and acoustic cavitation parameters such as frequency. Further investigations are being made into FC sonochemical kinetics concentration dependence and how chain length affects the dependence.

**Acknowledgment.** Research support and donation of analytical equipment from the 3M Environmental Laboratory is gratefully acknowledged. We also thank Jie Cheng and Dr. Hyungwoong Park for their useful discussions and Dr. Nathan Dalleska of the Environmental Analytical Center for analytical assistance.

## References and Notes

- (1) Key, B. D.; Howell, R. D.; Criddle, C. S. *Environ. Sci. Technol.* **1997**, *31*, 2445–2454.
- (2) 3M Company. *Docket AR226-0547*; Office of Pollution Prevention and Toxics; U.S. Environmental Protection Agency: Washington, DC, 1999.
- (3) Moody, C. A.; Field, J. A. *Environ. Sci. Technol.* **2000**, *34*, 3864–3870.
- (4) Kärman, A.; Ericson, I.; van Bavel, B.; Darnerud, P.; Aune, M.; Glynn, A.; Lignell, S.; Lindström, G. *Environ. Health Persp.* **2007**, *115*, 226–230.
- (5) Jones, P. D.; Hu, W.; Coen, W. D.; Newsted, J. L.; Giesy, J. P. *Environ. Toxicol. Chem.* **2003**, *22*, 2639–2649.
- (6) Russell, M. H.; Berti, W. R.; Szostek, B.; Buck, R. C. *Environ. Sci. Technol.* **2008**, *42*, 800–807.
- (7) Van de Vijver, K. I.; Hoff, P.; Das, K.; Brasseur, S.; van Dongen, W.; Esmans, E.; Reijnders, P.; Blust, R.; De Coen, W. *Environ. Sci. Technol.* **2005**, *39*, 6978–6984.
- (8) 3M Company. *Docket AR226-0588*; Office of Pollution Prevention and Toxics; U.S. Environmental Protection Agency: Washington, DC, 1999.

- (9) Chang, S.; Das, K.; Ehresman, D. J.; Ellefson, M. E.; Gorman, G. S.; Hart, J. A.; Noker, P. E.; Tan, U.; Lieder, P. H.; Lau, C.; Olsen, G. W.; Butenhoff, J. L. *Toxicol. Sci.* **2008**, *104*, 40–53.
- (10) NICNAS, 2005. *Potassium perfluorobutanesulfonate. Existing chemical hazard assessment report*. Department of Health and Aging, National Industrial Chemical Notification and Assessment Scheme (NICNAS). Australian Government, Sydney, NSW, Australia.
- (11) Ochoa-Herrera, V.; Sierra-Alvarez, R. *Chemosphere* **2008**, *72*, 1588–1593.
- (12) 3M Company. *Docket AR226-1699*; Office of Pollution Prevention and Toxics; U.S. Environmental Protection Agency: Washington, DC, 1999.
- (13) Oliyai, F.; Kriens, D.; Kessler, K. Report to Senate Environment Committee, 2006.
- (14) *CRC Handbook of Chemistry and Physics*, 61st ed.; CRC Press, Inc.: Boca Raton, FL, 1980.
- (15) Hudlicky, M.; Pavlath, A. E. *Chemistry of Organic Fluorine Compounds II: A Critical Review*; American Chemical Society: Washington, DC, 1995.
- (16) Moriawaki, H.; Takagi, Y.; Tanaka, M.; Tsuruho, K.; Okitsu, K.; Maeda, Y. *Environ. Sci. Technol.* **2005**, *39*, 3388–3392.
- (17) Vecitis, C. D.; Park, H. P.; Cheng, J.; Mader, B. T.; Hoffmann, M. R. *J. Phys. Chem. A* **2008**, *112*, 4261–4270.
- (18) Petrier, C.; Francony, A. *Water Sci. Technol.* **1997**, *35*, 175–180.
- (19) Theron, P.; Pichat, P.; Guillard, C.; Petrier, C.; Chopin, T. *Phys. Chem. Chem. Phys.* **1999**, *4*, 4663–4668.
- (20) Colussi, A. J.; Weavers, L. K.; Hoffmann, M. R. *J. Phys. Chem. A* **1998**, *102*, 6927–6934.
- (21) Leighton, T. G. *The Acoustic Bubble*; Academic Press: London, 1994.
- (22) Suslick, K. S.; Hammerton, D. A.; Cline, R. E. *J. Am. Chem. Soc.* **1986**, *108*, 5641–5642.
- (23) Destailats, H.; Hung, H.; Hoffmann, M. R. *Environ. Sci. Technol.* **2000**, *34*, 311–317.
- (24) Hung, H.; Hoffmann, M. R. *J. Phys. Chem. A* **1999**, *103*, 2734–2739.
- (25) Kotronoreau, A.; Mills, G.; Hoffmann, M. R. *J. Phys. Chem.* **1991**, *95*, 3630–3638.
- (26) Hua, I.; Hoffmann, M. R. *Environ. Sci. Technol.* **1997**, *31*, 2237–2243.
- (27) Sostaric, J. Z.; Riesz, P. *J. Phys. Chem. B* **2002**, *106*, 12537–12548.
- (28) Tronson, R.; Ashokumar, M.; Grieser, F. *J. Phys. Chem. B* **2003**, *107*, 7307–7311.
- (29) Fyrrillas, M.; Szeri, A. J. *J. Fluid Mech.* **1996**, *311*, 361–378.
- (30) Sostaric, J. Z.; Riesz, P. *J. Am. Chem. Soc.* **2001**, *123*, 11010–11019.
- (31) Ashokumar, M.; Hodnett, M.; Zeqiri, B.; Grieser, F.; Price, G. J. *J. Am. Chem. Soc.* **2007**, *129*, 2250–2258.
- (32) Vecitis, C. D.; Park, H. P.; Cheng, J.; Mader, B. T.; Hoffmann, M. R. *J. Phys. Chem. C* **2008**, *112*, 16850–16857.
- (33) Cheng, J.; Vecitis, C. D.; Park, H.; Mader, B. T.; Hoffmann, M. R. *Environ. Sci. Technol.* **2008**, *42*, 8057–8063.
- (34) Markham, G. D.; Bock, C. L.; Bock, C. W. *Struct. Chem.* **1997**, *8*, 293–307.
- (35) Guthrie, J. P.; Stein, A. R.; Huntington, A. P. *Can. J. Chem.* **1998**, *76*, 929–936.
- (36) Israelachvili, J. N.; *Intermolecular and Surface Forces: Applications to Colloidal and Biological Systems*; Academic Press: Orlando, FL, 1985.
- (37) Simister, E. A.; Lee, E. M.; Lu, J. R.; Thomas, R. K.; Ottewill, R. H.; Rennie, A. R.; Penfold, J. J. *Chem. Soc., Faraday Trans.* **1992**, *88*, 3033–3041.
- (38) Zhang, G.; Hua, I. *Environ. Sci. Technol.* **2000**, *34*, 1529–1534.
- (39) Colussi, A. J.; Hung, H.; Hoffmann, M. R. *J. Phys. Chem. A* **1999**, *103*, 2696–2699.
- (40) Okitsu, K.; Ashokumar, M.; Grieser, F. *J. Phys. Chem.* **2005**, *109*, 20673–20675.
- (41) Wayment, D. G.; Casadonte, D. J. *Ultrason. Sonochem.* **2002**, *9*, 189–195.
- (42) Ciawi, E.; Rae, J.; Ashokumar, M.; Grieser, F. *J. Phys. Chem. B* **2006**, *110*, 13656–13660.
- (43) Price, G.; Ashokumar, M.; Grieser, F. *J. Am. Chem. Soc.* **2004**, *126*, 2755–2762.
- (44) Beckett, M. A.; Hua, I. *J. Phys. Chem. A* **2001**, *105*, 3796–3802.
- (45) Petrier, C.; David, B.; Laguian, S. *Chemosphere* **1996**, *32*, 1709–1718.
- (46) Alegria, A.; Lion, Y.; Kondo, T.; Riesz, P. *J. Phys. Chem.* **1989**, *93*, 4909–4913.
- (47) Okitsu, K.; Suzuki, T.; Takenaka, N.; Bandow, H.; Nishimura, R.; Maeda, Y. *J. Phys. Chem. B* **2006**, *110*, 20081–20084.
- (48) Eller, A.; Flynn, H. G. *J. Acoust. Soc. Am.* **1965**, *37*, 493–503.
- (49) Ruiz, A. I.; Canals, A.; Hernandez, V. *J. Anal. At. Spectrosc.* **1993**, *8*, 109–113.
- (50) Mackay, D.; Shiu, W. Y.; Ma, K. C. *Illustrated Handbook of Physical-Chemical Properties and Environmental Fate of Organic Chemicals*; Lewis Publishers: Boca Raton, FL, 1993; Vol. III.
- (51) Cheng, J. Y.; Riesz, P. *Ultrason. Sonochem.* **2007**, *14*, 667–671.
- (52) Langmuir, I. *J. Am. Chem. Soc.* **1916**, *38*, 2221.
- (53) Glockner, V.; Lunkwitz, K.; Prescher, D. *Tenside Surf. Det.* **1989**, *26*, 6.
- (54) Fainerman, V. B. *Colloids Surf.* **1991**, *57*, 249–266.
- (55) Chang, C. H.; Franses, E. I. *Colloid Surf. A* **1995**, *100*, 1–45.
- (56) Goss, K. *Environ. Sci. Technol.* **2008**, *42*, 456–458.
- (57) Heckster, F. M.; Laane, R.; deVoogt, P. *Rev. Environ. Contam. Toxicol.* **2003**, *179*, 99–121.
- (58) Environment Agency. *Environmental Risk Evaluation Report: Perfluorooctane sulphonate (PFOS)*; Chemical Assessment Section: Wallingford, United Kingdom, 2004.

JP903003W